ring atoms in the singlet ground state of *p*-dioxyne. This value is substantially larger than the calculated (0.04 kcal/mol) energy difference between the planar (C_{2v}) and folded (C_s) structures of singlet cyclopentyne. Interestingly, from the relative energies given in Table II, it is found that at the GVB/3-21G level the $^1A_1$ singlet state, which is the planar form of the singlet ground state of *p*-dioxyne, lies 14.6 kcal/mol *below* the corresponding planar triplet state ($^3B_2$). This prediction is consistent with the relative singlet-triplet energy ordering found for the equilibrium structures (C_2) of these states.

Since it is plausible that the most promising technique for the identification of singlet *p*-dioxyne in the near future will be the infrared matrix spectroscopy, we turn our attention to the calculated C≡C stretching frequency for this species. It should be noted here that the 3-21G SCF harmonic frequencies are expected to be of the order of 11% higher than the experimental frequencies.[27] Therefore, an empirical correction of 11% would reduce the calculated C≡C stretching frequency in singlet *p*-dioxyne to 1897 cm^{-1}. Analogously, for the lowest triplet state (^3B) of *p*-dioxyne, a corrected C_2C_3 bond stretching frequency of 1659 cm^{-1} can be predicted. For comparison, the observed C=C stretching frequency[28] in the structurally related *p*-dioxene molecule is 1654 cm^{-1}. Consequently, strictly on the basis of these carbon-carbon bond stretching frequencies, we would conclude that the triplet *p*-dioxyne should be considered as a cycloalkene rather than a cycloalkyne. We hope that these frequencies will prove to be helpful in aiding the identification of these species.

(27) Pople, J. A.; Schlegel, H. B.; Krishnan, E.; DeFrees, D. J.; Binkley, J. S.; Frisch, M. J.; Whiteside, R. A.; Hout, R. F.; Hehre, W. J. *Int. J. Quantum Chem. Symp.* **1981**, *15*, 269.

(28) Measured by the authors (liquid film, NaCl) on a Perkin-Elmer 681 spectrophotometer.

IV. Conclusions

The following conclusions can be drawn from the calculations presented here. (1) The electronic ground state of *p*-dioxyne is a singlet state (^1A) which has a nonplanar (C_2) acetylenic structure. (2) Because of the considerable amount of diradical character exhibited by the ground-state singlet, the single configuration RHF approach predicts an artificial nonacetylenic Lewis structure for this state. (3) The lowest energy triplet state of *p*-dioxyne (^3B) is predicted to lie about 13 kcal/mol above the ground-state singlet and also has a nonplanar (C_2) structure with a normal carbon-carbon double bond in the ynedioxy moiety. (4) The triple-bond stretching frequency for singlet *p*-dioxyne is predicted to be 1897 cm^{-1}, while the double-bond stretching frequency for the triplet state is 1659 cm^{-1}.

Acknowledgment. The authors have benefited from several discussions with Professor Roald Hoffman during his visit to Barcelona. The calculations were carried out using the IBM 4341 computer at the "Centre d'Informàtica de la Universitat de Barcelona" and a DEC VAX 11-750 computer purchased with funds provided by the CAICYT (Grant No. 657/81). The GAMESS program was kindly made available by Dr. Michael L. Mckee. We are indebted to the referees for their useful remarks, which served to clarify various points in the initial manuscript.

Registry No. *p*-Dioxyne, 68997-21-7.

Supplementary Material Available: Cartesian coordinates of the optimized molecular structures (C_2 and C_{2v} symmetries) and harmonic frequencies and normal modes (in internal valence coordinates) for the ground-state singlet (at GVB/3-21G level of theory) and triplet (at UHF/3-21G level of theory) electronic states of *p*-dioxyne (16 pages). Ordering information is given on any current masthead page.

Insertion of Carbon Monoxide into the Sc-H Bond of Cl_2ScH

A. K. Rappé

Contribution from the Department of Chemistry, Colorado State University, Fort Collins, Colorado 80523. *Received February 5, 1987*

Abstract: Correlated ab initio theoretical calculations at the valence double-ζ plus polarization level are used to study the insertion of carbon monoxide into a scandium-hydrogen σ bond. We find a Lewis acid-Lewis base interaction between scandium and the carbon monoxide of 16.4 kcal/mol. The reaction occurs with a relatively small activation energy ($\Delta E^{\ddagger}$ = 23.7 kcal/mol with respect to the Lewis acid-base complex) leading to an η^2-formyl complex. The reaction is moderately exothermic (ΔE = −6.1 kcal/mol with respect to the Lewis acid-base complex). The explanation for the small barrier is precisely the same as for previously studied metallo 2 + 2 reactions. The effect of polarization functions and electron correlation on the position of the transition state and the exothermicity of the reaction were also studied.

Metalloformyl and acyl species are frequently invoked as key intermediates in the metal-catalyzed reduction of CO and the synthetically useful carbonylation reactions.[1] Despite η^1-acyls being rather common[1,2] there are relatively few examples of η^1-formyl complexes[3] and even fewer examples of direct insertion of CO into M-H bonds.[4] There are also few examples of η^2-formyl or -acyl species.[5] The rarity of these species has been attributed to either kinetic inaccessibility or thermodynamic instability.

Scheme I

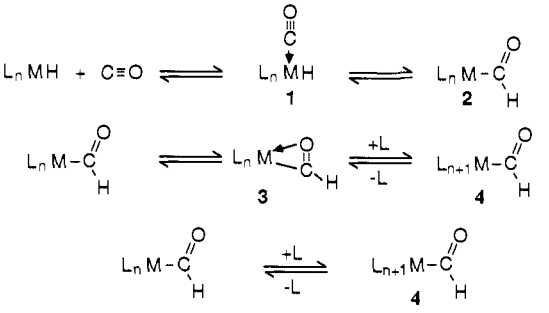

(1) Collman, J. P.; Hegedus, L. S. *Principles and Applications of Organotransition Metal Chemistry*; University Science Books: Mill Valley, CA, 1980.

(2) Tkatchenko, I., In *Comprehensive Organometallic Chemistry*; Wilkenson, G., Ed.; Pergamon Press: New York, 1982; Vol. 8, Chapter 50, pp 101-224.

(3) Gladysz, J. A. *Adv. Organomet. Chem.* **1982**, *20*, 1 and references therein.

(4) Farnos, M. D.; Woods, B. A.; Wayland, B. B. *J. Am. Chem. Soc.* **1986**, *108*, 3659-3663 and references therein.

0002-7863/87/1509-5605$01.50/0

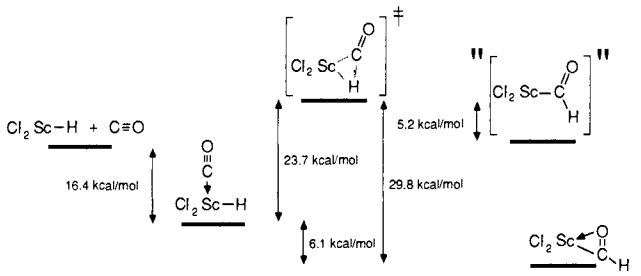

Figure 1. The reaction energy diagram for insertion of CO into the Sc–H σ bond of Cl_2ScH. The energies are obtained from the CI calculations.

A general scheme[1-13] for the reaction of a metal hydride with carbon monoxide consists of an initial complexation of carbon monoxide to a coordinatively unsaturated metal complex to form complex **1**. This complex undergoes an intramolecular rearrangement to form a coordinately unsaturated η^1-formyl complex **2**, which can further rearrange to form a (perhaps) transient η^2-formyl complex **3**. Then complex **3** or the unsaturated complex **2** reacts with added ligand to form the final saturated η^1-formyl complex **4**. This sequence is outlined in Scheme I. The relative energetics of the stable stationary states in this scheme are subject to influences from the metal and the ligands bonded to the metal. Complexes in which the η^1 form of the formyl or acyl is the observed entity are well documented[1-3] (usually group 6–10 metals). Complexes in which the η^2-formyl or acyl is the stable form are also known[5] (group 4–6 metals). The relative energetics of the transition states are also subject to influences from the metal and the ligands bonded to the metal. Most metal hydrides are either kinetically or thermodynamically inert to reaction with carbon monoxide.[1] However, there are reports of hydrides that do react with carbon monoxide either directly or through a radical pathway.[4,6]

As a first step in the ab initio characterization of the relative energetics of η^1- and η^2-acyl and -formyl complexes, as well as the transition states interconnecting them, we have characterized the reaction coordinate for the insertion of CO into the Sc–H bond of Cl_2ScH. This system was chosen for our initial study because of its relative simplicity—there are no additional ligands in the H–C–O plane and there are no nonbonding d electrons to complicate the metal–ligand bonding interactions. Further, recent theoretical work on group 4 and group 6 η^2-acyl and -formyl complexes[7-10] has suggested that η^1-acyl species are stationary states on the same potential energy surface as η^2-acyls. Finally, this ligand set has been used for several other theoretical studies on related organometallic reactions.[14]

We will first discuss the energetic profile along the reaction coordinate obtained with analytic Hartree–Fock gradients. The electronic structures of the stationary points along this reaction coordinate are presented next in section II. A comparison with previous work is given in section III. The overall conclusions are given in section IV, and the theoretical details are given in section V.

Table I. Molecular Coordinates and CI Total Energies[a]

atom	X	Y	Z
(a) Cl_2ScH·CO CI Total Energy = −1078.618599			
Sc	0.0	−0.468 992 075	−0.246 103 39
C11	−2.136 511 37	0.258 563 589	−0.928 218 647
C12	2.136 511 37	0.258 563 589	−0.928 218 647
H	0.0	−1.959 172 92	0.690 486 857
C	0.0	0.143 309 661	2.080 966 82
O	0.0	0.187 742 764	3.199 450 57
(b) $Cl_2Sc(\eta^2$-HCO) CI Total Energy = −1078.630387			
Sc	0.0	0.010 521 088	0.147 162 426
C11	−2.064 551 96	−0.014 461 787	−0.993 800 315
C12	2.064 551 96	−0.014 461 787	−0.993 800 315
H	0.0	−1.073 302 26	3.234 053 32
C	0.0	−0.665 164 558	2.237 091 65
O	0.0	0.601 503 130	2.107 622 73
(c) Cl_2ScHCO Transition-State CI Total Energy = −1078.583760			
Sc	0.0	−0.042 624 323	−0.246 103 139
C11	−2.130 955 26	0.035 215 583	−1.058 817 44
C12	2.130 955 26	0.035 215 583	−1.058 817 44
H	0.0	−1.350 482 49	1.867 921 37
C	0.0	−0.187 162 977	2.071 481 05
O	0.0	0.189 289 056	3.207 848 85
(d) "$Cl_2Sc(\eta^1$-HCO)" CI Total Energy = −1078.591141			
Sc	0.0	0.149 544 227	−0.027 996 18
C11	−2.120 679 26	−0.046 377 063	−1.028 467 25
C12	2.120 679 26	−0.046 377 063	−1.028 467 25
H	0.0	−1.626 504 09	1.867 921 37
C	0.0	−0.187 162 977	2.282 349 53
O	0.0	0.303 151 250	2.942 456 20

[a] Coordinates are in Å and energies in hartrees.

I. Reaction Coordinate

The reaction coordinate found for the reaction of Cl_2ScH with CO is qualitatively quite different from that outlined in Scheme I (see Figure 1). We find only two stable stationary states: the initial Lewis acid–Lewis base complex and the final η^2-formyl species. We are not considering addition of ligand to form a saturated complex in this study. Of particular significance is that there is no stationary state on the potential surface corresponding to an η^1-formyl species. The hypothetical η^1-formyl species is found to lie *along* the reaction coordinate connecting reactants and products—that is, it does not possess zero gradient. As discussed below in section V, starting from a reasonable η^1-formyl geometry the molecule is unstable with respect to distortion either to the insertion transition state or to the η^2-formyl. The calculated barrier for the overall reaction from the lewis acid–base complex is relatively small (23.7 kcal/mol), as found experimentally[1-6] and theoretically[7-13] for related systems (see section III). The ex-

(5) Fachinetti, G.; Floriani, C.; Marchetti, F.; Medino, S. *J. Chem. Soc., Chem. Commun.* **1976**, 522. Fachinetti, G.; Fochi, G.; Floriani, C. *J. Chem. Soc., Dalton Trans.* **1977**, 1946. Fachinetti, G.; Floriani, C.; Stockli-Evans, H. *Ibid.* **1977**, 2297. Erker, G.; Rosenfeldt, F. *Angew. Chem., Int. Ed. Engl.* **1978**, *17*, 605. Marsella, J. A.; Caulton, K. G. *J. Am. Chem. Soc.* **1980**, *102*, 1747. Erker, G.; Rseonfeldt, F. *J. Organomet. Chem.* **1980**, *188*, C1. Pearson, R. G.; Walker, H. W.; Mauermann, H.; Ford, P. C. Inorg. Chem. **1981**, *20*, 2743. Strauss, O. A.; Grubbs, R. H. *J. Am. Chem. Soc.* **1982**, *104*, 5499. Marsella, J. A.; Huffman, J. C.; Caulton, K. G.; Longato, B.; Norton, J. R. *Ibid.* **1982**, *104*, 6360. Labinger, J. A.; Miller, J. S. *Ibid.* **1982**, *104*, 6856. Floriani, C. *Pure Appl. Chem.* **1983**, *55*, 1–10. Moore, E. J.; Straus, D. A.; Armantrout, J.; Santarsiero, B. D.; Grubbs, R. H.; Bercaw, J. E. *J. Am. Chem. Soc.* **1983**, *105*, 2068. Belmonte, P. A.; Cloke, F. G. N.; Schrock, R. R. *Ibid.* **1983**, *105*, 2643. Kropp, K.; Skilbe, V.; Erker, G.; Krüger, C. *Ibid.* **1983**, *105*, 3353. Sonnenberger, D. C.; Mintz, E. A.; Marks, T. J. *Ibid.* **1984**, *106*, 3484. Moloy, K. G.; Marks, T. J. *Ibid.* **1984**, *106*, 7051. Fanwick, P. E.; Kobriger, L. M.; McMullen, A. K.; Rothwell, I. P. *J. Am. Chem. Soc.* **1986**, *108*, 8095–8097.

(6) Paonessa, R. S.; Thomas, N. C.; Halpern, J. *J. Am. Chem. Soc.* **1985**, *107*, 4333.

(7) Berke, H.; Hoffmann, R. *J. Am. Chem. Soc.* **1978**, *100*, 7224–7236.

(8) Hofmann, P.; Stauffert, P.; Tatsumi, K.; Nakamura, A.; Hoffmann, R. *Organometallics* **1985**, *4*, 404–406. Tatsumi, K.; Nakamura, A.; Hofmann, P.; Stauffert, P.; Hoffmann, R. *J. Am. Chem. Soc.* **1985**, *107*, 4440–4451.

(9) Ziegler, T.; Versluis, L.; Tschinke, V. *J. Am. Chem. Soc.* **1986**, *108*, 612–617.

(10) Curtis, M. D.; Shiu, K.-B.; Butler, W. M. *J. Am. Chem. Soc.* **1986**, *108*, 1550–1561.

(11) Sakaki, S.; Kitaura, K.; Morokuma, K.; Ohkubo, K. *J Am. Chem. Soc.* **1983**, *105*, 2280–2286.

(12) Koga, N.; Morokuma, K. *J. Am. Chem. Soc.* **1985**, *107*, 7230–7231.

(13) Nakamura, S.; Dedieu, A. *Chem. Phys. Lett.* **1984**, *111*, 243–248. Dedieu, A.; Nakamura, S. In "Quantum Chemistry: The Challange of Transition Metals and Coordination Chemistry": Veillard, A., Ed. *NATO ASI Ser. C* Vol. 176 p 277 (1985). Dedieu, A.; Sakaki, S.; Strich, A.; Siegbahn, P. E. M. *Chem. Phys. Lett.*, in press.

(14) Steigerwald, M. L.; Goddard, W. A. *J. Am. Chem. Soc.* **1984**, *106*, 308–311. Rappé, A. K.; Upton, T. H. *Organometallics* **1984**, *3*, 1440–1442. Upton, T. H.; Rappé, A. K. *J. Am. Chem. Soc.* **1985**, *107*, 1206–1218. Fujimoto, H.; Yamasaki, T.; Mizutani, H.; Koga, N. *Ibid.* **1985**, *107*, 6157–6161. Koga, N.; Obara, S.; Kitaura, K.; Morokuma, K. *Ibid.* **1985**, *107*, 7109–7116. Rabaâ, H.; Sailard, J.-Y.; Hoffmann, R. *Ibid.* **1986**, *108*, 4327–4333.

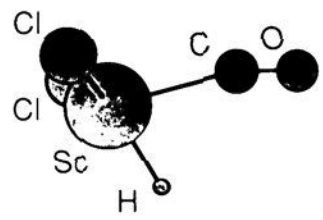

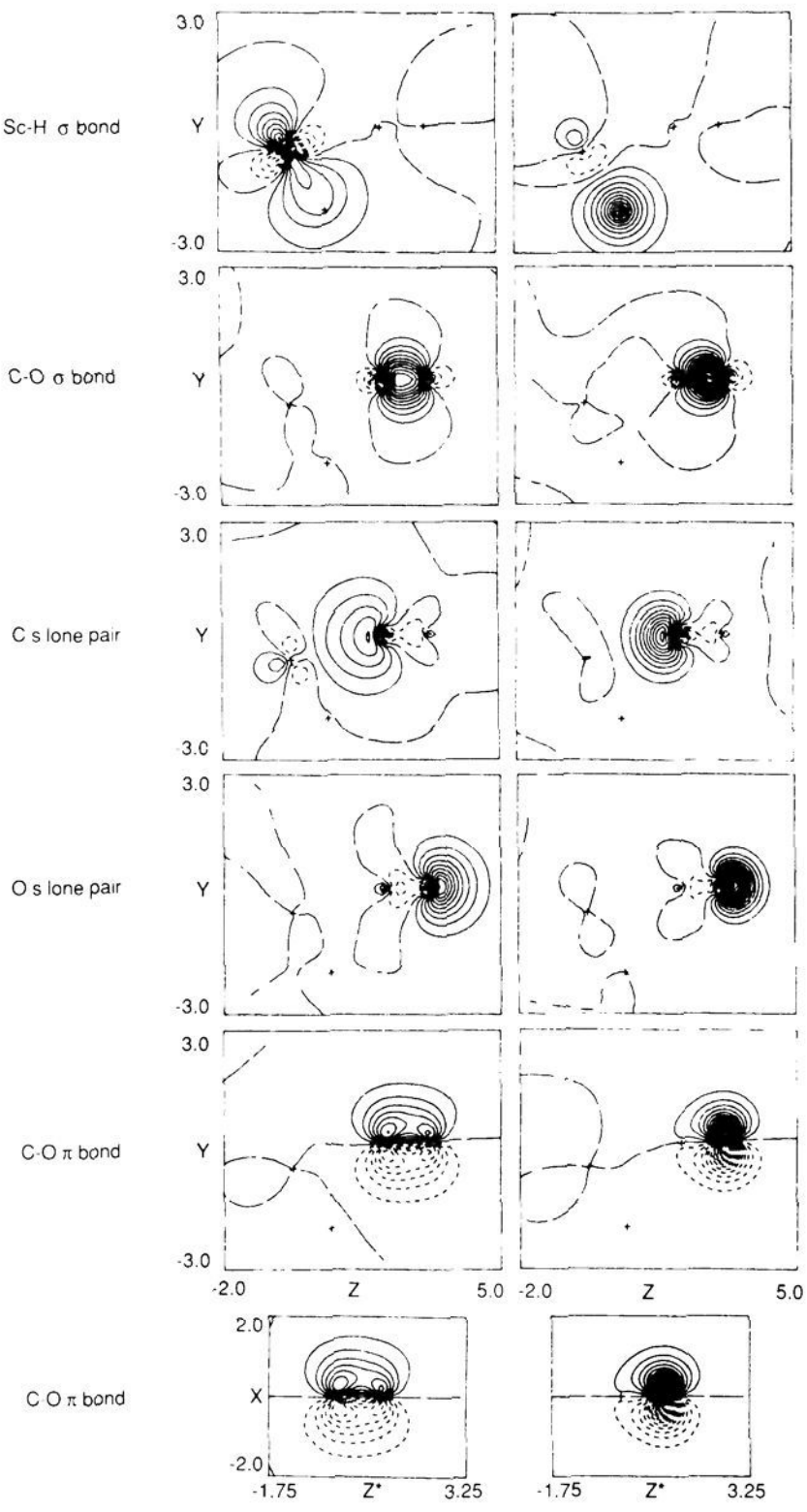

Figure 2. Contour plots of the GVB orbitals defining the valence space for CO interacting weakly with Cl_2ScH. The plotting plane for the first five rows contains scandium, hydrogen, carbon, and oxygen. The plotting plane for the last row contains the x coordinate and the carbon–oxygen bond vector. The solid contours define positive orbital amplitude (spaced 0.05 au), the dashed contours define negative orbital amplitude, and the long dashed lines define nodal lines. The Sc–H σ bond is plotted in the top row, the C–O σ bond is plotted in the second row, C and O s lone pairs are plotted in the third and fourth rows, respectively, and the C–O π bonds are plotted in the fifth and sixth rows.

planation for the small barrier has been previously discussed[14] and will be summarized in section II.D below.

II. Electronic Structures

We begin by considering the reactant limit (free CO plus Cl_2ScH) and the product limit (an η^2-formyl) in subsections A and B, respectively. In subsection C we consider the electronic structure of the saddle point connecting the limits and related η^1-formyl. In subsection D we examine the orbital changes that occur in going from the reactants to the transition state. Finally, the electronic changes that occur in going from the transition state

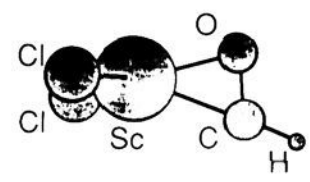

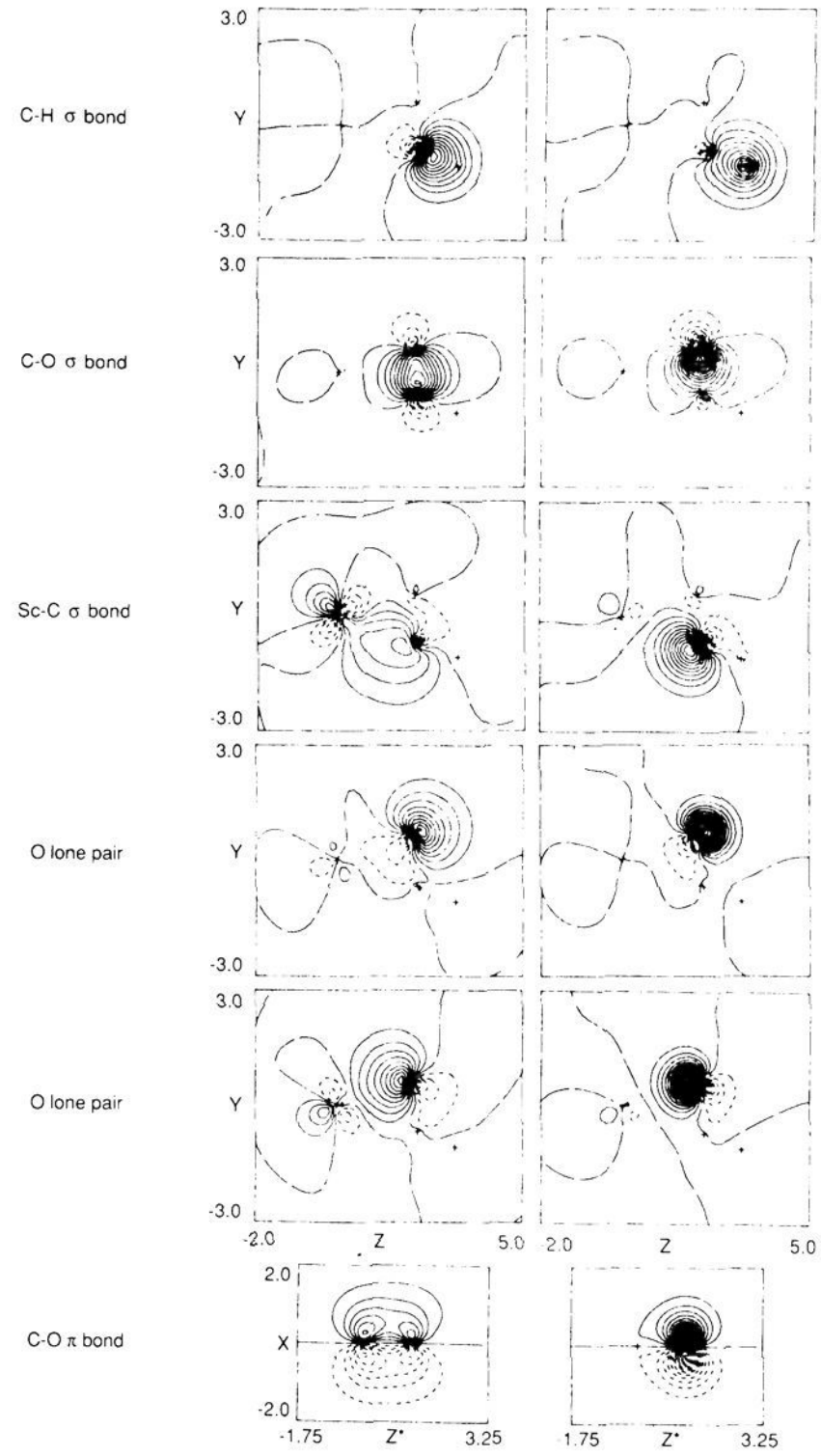

Figure 3. Contour plots of the GVB orbitals defining the valence space for the η^2-formyl form of Cl_2ScHCO. The plotting plane and contours are as defined in Figure 2. The C–H σ bond is plotted in the top row, the C–O σ bond is plotted in the second row, the Sc–C σ bond is plotted in the third row, the noninteracting O lone pair is plotted in the fourth row, the O lone pair participating in a dative interaction with Sc is plotted in the fifth row, and the C–O π bond is plotted in the sixth row.

(very nearly an η^1-formyl) to the final η^2-formyl product are discussed in subsection E.

A. CO plus Cl_2ScH. The generalized valence bond (GVB) descriptions of the electronic structures of carbon monoxide[15] and a Sc–H σ bond[16] have been discussed previously. The valence orbitals of carbon monoxide interacting weakly with Cl_2ScH are presented in Figure 2. Briefly, the Sc–H σ bond of Cl_2ScH as shown in row 1 of Figure 2 consists of a covalent bonding interaction between the s orbital of hydrogen and a d_σ orbital on Sc. The carbon–oxygen valence orbitals consist of a largely donor acceptor σ bond (donation from oxygen to carbon) shown in row

(15) Rappé, A. K.; Goddard, W. A. *J. Am. Chem. Soc.* **1982**, *104*, 448–456; 3287–3294.

(16) Steigerwald, M. L.; Goddard, W. A. *J. Am. Chem. Soc.* **1984**, *106*, 308–311.

Table II. Major Bond Distances and Bond Angles[a]

	(a) $Cl_2ScH{\cdot}CO$		
Sc–Cl	2.358	Cl–Sc–Cl	129.95
Sc–H	1.760	H–Sc–C	72.59
Sc–C	2.406	H–C–Sc	41.78
C–H	2.521	Sc–C–O	167.53
C–O	1.119	H–C–O	125.75
	(b) $Cl_2Sc(\eta^2\text{-HCO})$		
Sc–Cl	2.359	Cl–Sc–Cl	122.13
Sc–H	3.272	O–Sc–C	34.69
Sc–C	2.196	H–Sc–C	1.43
Sc–O	2.048	H–C–Sc	175.65
C–H	1.077	Sc–C–O	66.25
C–O	1.273	H–C–O	118.10
	(c) Cl_2ScHCO Transition State		
Sc–Cl	2.352	Cl–Sc–Cl	129.95
Sc–H	2.335	H–Sc–C	30.19
Sc–C	2.143	H–C–Sc	83.94
C–H	1.181	Sc–C–O	157.80
C–O	1.197	H–C–O	118.25
	(d) "$Cl_2Sc(\eta^1\text{-HCO})$"		
Sc–Cl	2.353	Cl–Sc–Cl	128.65
Sc–C	2.208	H–C–Sc	120.0
C–H	1.095	Sc–C–O	117.13
C–O	1.226	H–C–O	122.87

[a] Bond distances in Å and band angles in deg.

2 of Figure 2, s lone pairs on carbon and oxygen shown in rows 3 and 4, respectively, of Figure 2, and two polar covalent π bonds (shown in rows 5 and 6 of Figure 2). The coordinates for this structure are given in Table Ia, and several bond distances and bond angles are in Table IIa.

B. η^2-Formyl. The six valence GVB orbitals of the η^2-formyl complex (shown in Figure 3) are quite analogous to the GVB orbitals of ethylene bound to Cl_2Ti.[17] That is, the Sc, C, and O form a pseudometallacycle consisting of a Sc–C σ bond (row 3 of Figure 3), a C–O σ bond (row 2 of Figure 3), and a Sc–O donor–acceptor bond involving an O lone pair and an empty d orbital of Sc (row 5 of Figure 3). In addition, the C–H σ bond is shown in row 1, and the remaining O lone pair is plotted in row 4 of Figure 3. The π bond between C and O is shown in row 6 of Figure 3. The metal–ligand bonds of the pseudometallacycle ring are somewhat strained as evidenced by the bonds not being directed along the bond axes. The d orbitals on scandium are not capable of being compressed to the angle of only 34.7°. This was previously observed by Steigerwald and Goddard for the related titanacyclopropane.[17] Though the σ orbitals might suggest significant participation by the carbene resonance structure **5** in addition to the formyl resonance structure **6**, the π bond is essentially that of formaldehyde and resonance structure **6** is dominant. From the plots in row 6 of Figure 3 one can see that the

5 **6**

C–O π bond is polarized substantially onto oxygen, suggesting that nucleophilic attack should occur at carbon; this is in agreement with experiment and previous theoretical work. The coordinates for this structure are given in Table 1b, and several bond distances and bond angles are in Table IIb.

C. The Saddle Point and η^1-Formyl Structures. The electronic structure of the transition state (see Figure 4) is quite similar to what would be expected for an η^1-formyl (see Figure 5). There are two equivalent oxygen lone pairs (rows 4 and 5 of Figures 4 and 5), C–H and C–C σ bonds (rows 1 and 2, respectively, of Figures 4 and 5), a Sc–C σ bond (row 3 of Figures 4 and 5), and a C–O σ bond (row 6 of Figures 4 and 5). The coordinates for

(17) Steigerwald, M. L.; Goddard, W. A. *J. Am. Chem. Soc.* **1985**, *107*, 5027–5035.

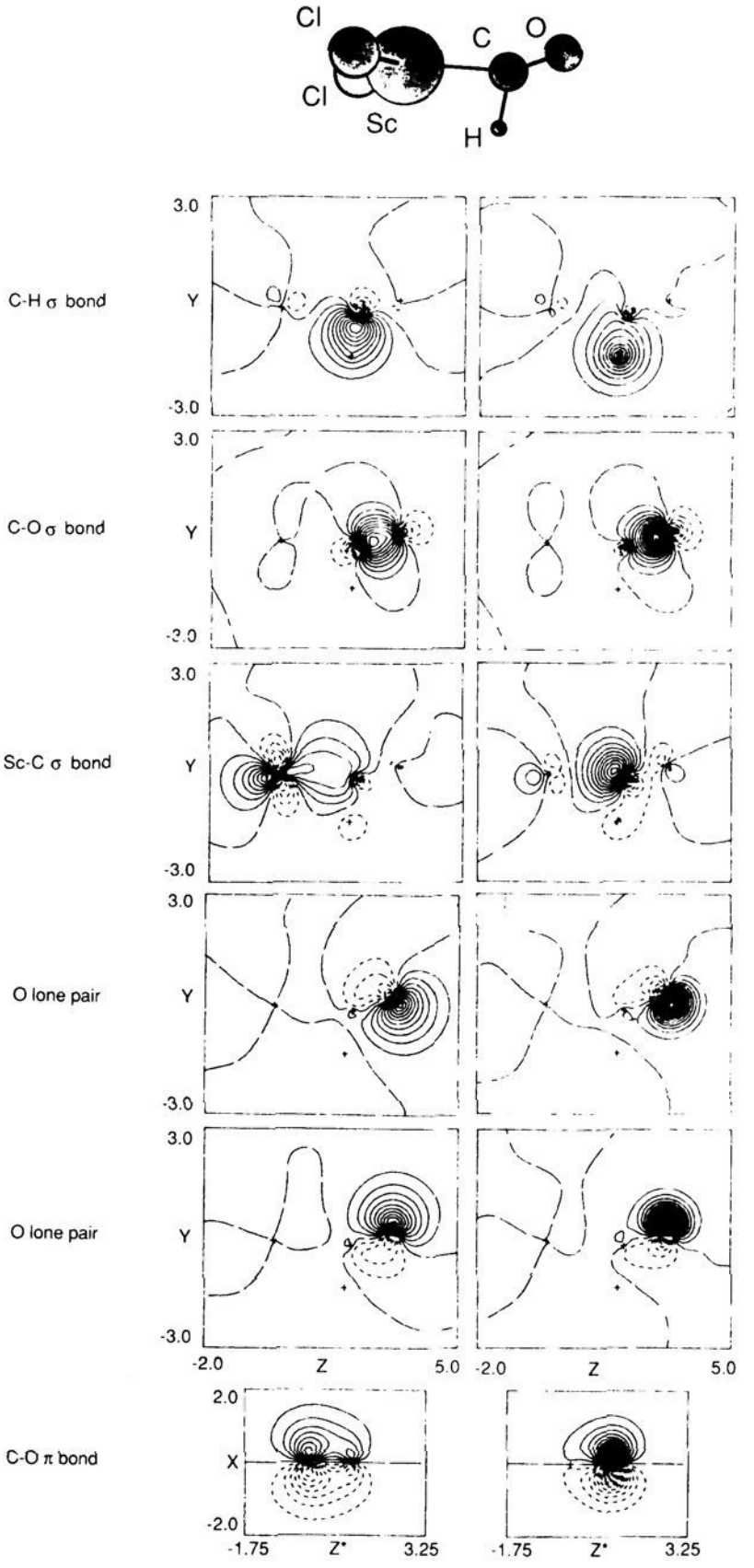

Figure 4. Contour plots of the GVB orbitals defining the valence space for the transition state interconnecting the reactant (plotted in Figure 2) and the product η^2-formyl (plotted in Figure 3). The plotting plane and contours are as defined in Figure 2. The C–H σ bond is plotted in the top row, the C–O σ bond is plotted in the second row, the Sc–C σ bond is plotted in the third row, the O lone pairs are plotted in the fourth and fifth rows, and the C–O π bond is plotted in the sixth row.

these structures are given in Table I, c and d, and several bond distances and bond angles are in Table II, c and d, for the saddle point and the hypothetical η^1-formyl structures, respectively.

D. Reaction Coordinate Connecting the Reactant and the Saddle Point. As can be seen from a comparison of Figures 2 and 4 there is significant change in each of the valence orbitals in going from reactant to transition state. The evolution of each orbital will be discussed separately. The most extensive reorganization occurs between the C s lone pair and the Sc–H σ bond. The electronic rearrangement which occurs here is quite analogous to that seen previously for four-center 2 + 2 reactions.[14]

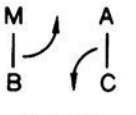

For the present three-center 2 + 2 case, there are energetic and electronic structural differences because one of the two active

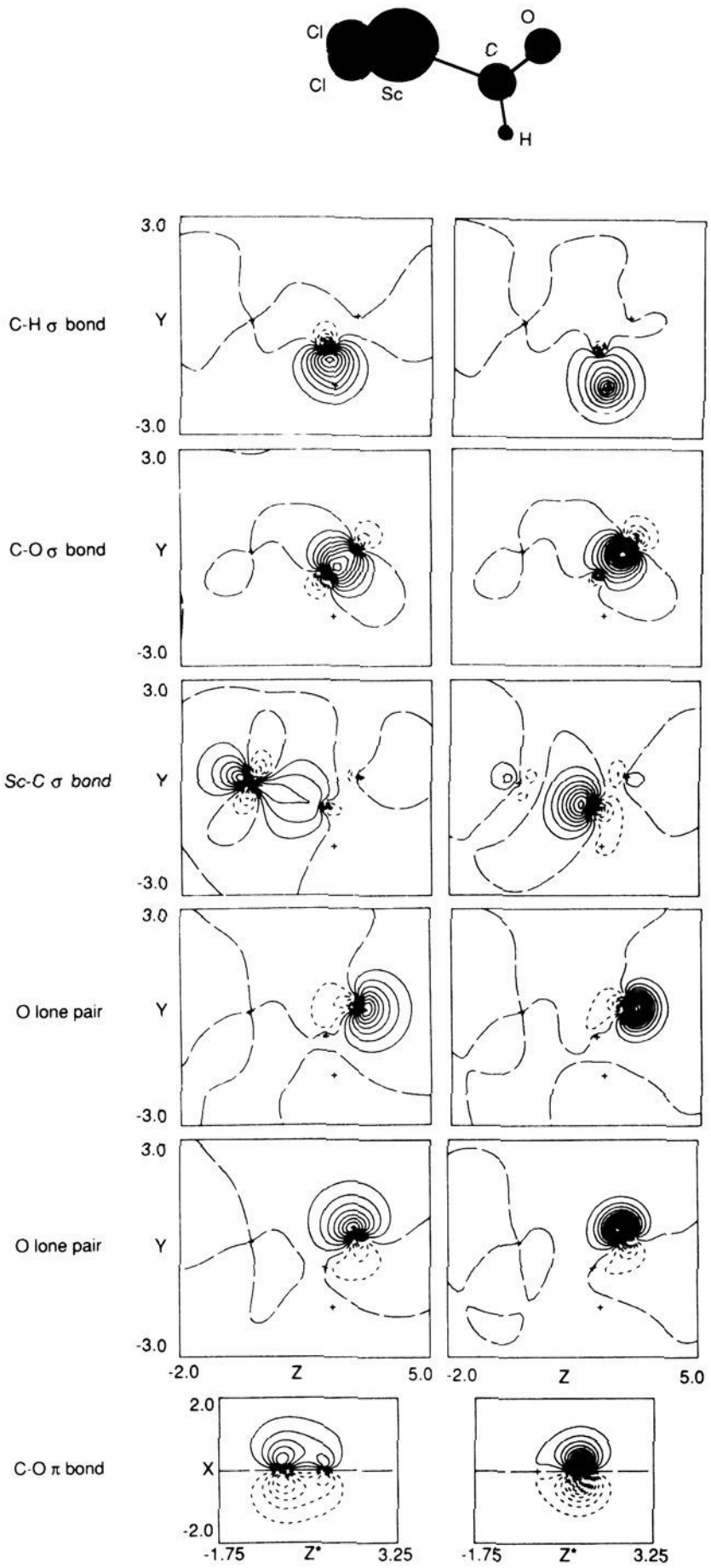

Figure 5. Contour plots of the GVB orbitals defining the valence space for the hypothetical η^1-formyl. The plotting plane and contours are as defined in Figure 2. The C–H σ bond is plotted in the top row, the C–O σ bond is plotted in the second row, the Sc–C σ bond is plotted in the third row, the O lone pairs are plotted in the fourth and fifth rows, and the C–O π bond is plotted in the sixth row.

electron pairs is concentrated on a single center. The electron motion is, however, quite analogous (see Figures 6 and 7).

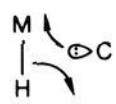

The major consequence of one of the two electron pairs of electrons being localized on a single center is that the orthogonality constraints dominant in the four-center case are not as demanding here since the two electron pairs are inherently further apart. The current reaction does have a higher calculated barrier than the 4-center 4-electron cases previously studied.[14] However, rather than think of the larger barrier being due to orthogonality constraints and avoided crossings, we believe that because of the

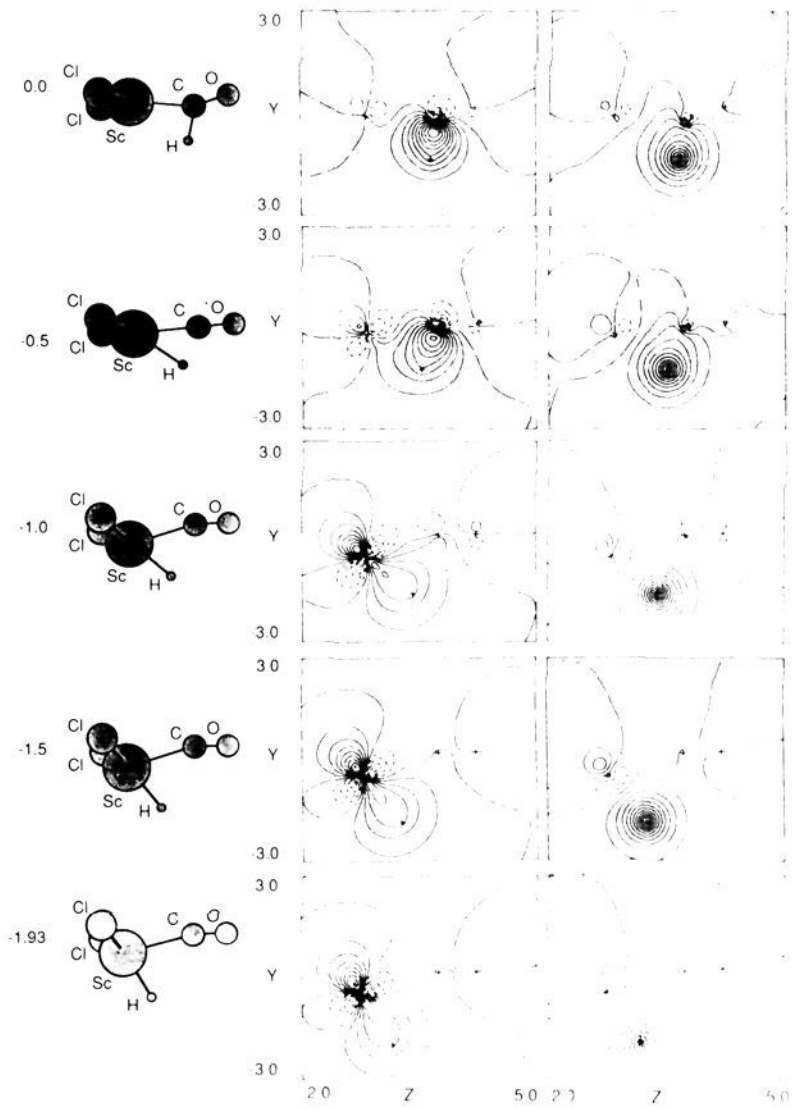

Figure 6. Contour plots of the GVB orbitals describing the formation of the Sc–C σ bond for the reaction coordinate connecting the reactant (plotted in Figure 2) and the transition state (plotted in Figure 4). The plotting plane and contours are as defined in Figure 2. The transition-state pair is plotted in the top row, the reactant pair is plotted in the last row, and points at 0.5-Å steps along the reaction coordinate are plotted in between.

endothermicity of the η^1-formyl, because the reaction is electronically favorable,[7-14] and because of the exothermicity of the reaction connecting the η^1-formyl and η^2-formyl species the barrier connecting the reactant and the η^1-formyl has nearly vanished and the barrier connecting the η^1-formyl and the η^2-formyl has vanished. That is, the usual reaction coordinate in Figure 8a is replaced by the reaction coordinate in Figure 8b.

The bottom row of Figure 6 shows the reactant Sc–H σ bond unperturbed by the C lone pair, shown in the bottom row of Figure 7. Note that there is only slight delocalization of the C lone pair into an empty d orbital on scandium. As one proceeds up the rows in Figures 6 and 7 the delocalization occurs smoothly; the Sc–H σ bond turns into a C–H σ bond and the C lone pair becomes a Sc–C σ bond though it is not directed along the Sc–C bond axis.

The C–O σ bond is essentially unperturbed during the reaction (see Figure 9). The O s lone pair and in-plane π bond mix substantially during the course of the reaction forming two equivalent hybridized oxygen lone pairs at the saddle point (see Figures 10 and 11). The C–O π bond in the plane perpendicular to the Sc–H–C–O plane changes only slightly during the course of the reaction—becoming more covalent (see Figure 12). Note the concentration of the orbital in column 1 of Figure 12 onto the carbon as the reaction proceeds.

E. Reaction Coordinate Connecting the Saddle Point and the η^2-Formyl Product. As can been seen from a comparison of Figures 3 and 4 there are only a few significant structure changes in going from the transition state to the final η^2-formyl product. One apparent change is the increasing donation from one of the formyl lone pairs into an empty d_σ orbital on scandium (see Figure 13). This interaction is what prevents the saddle point from simply relaxing into an η^1-formyl structure. The other significant change going from the transition state to the product occurs in the C–O π bond which becomes less covalent; note the increased delo-

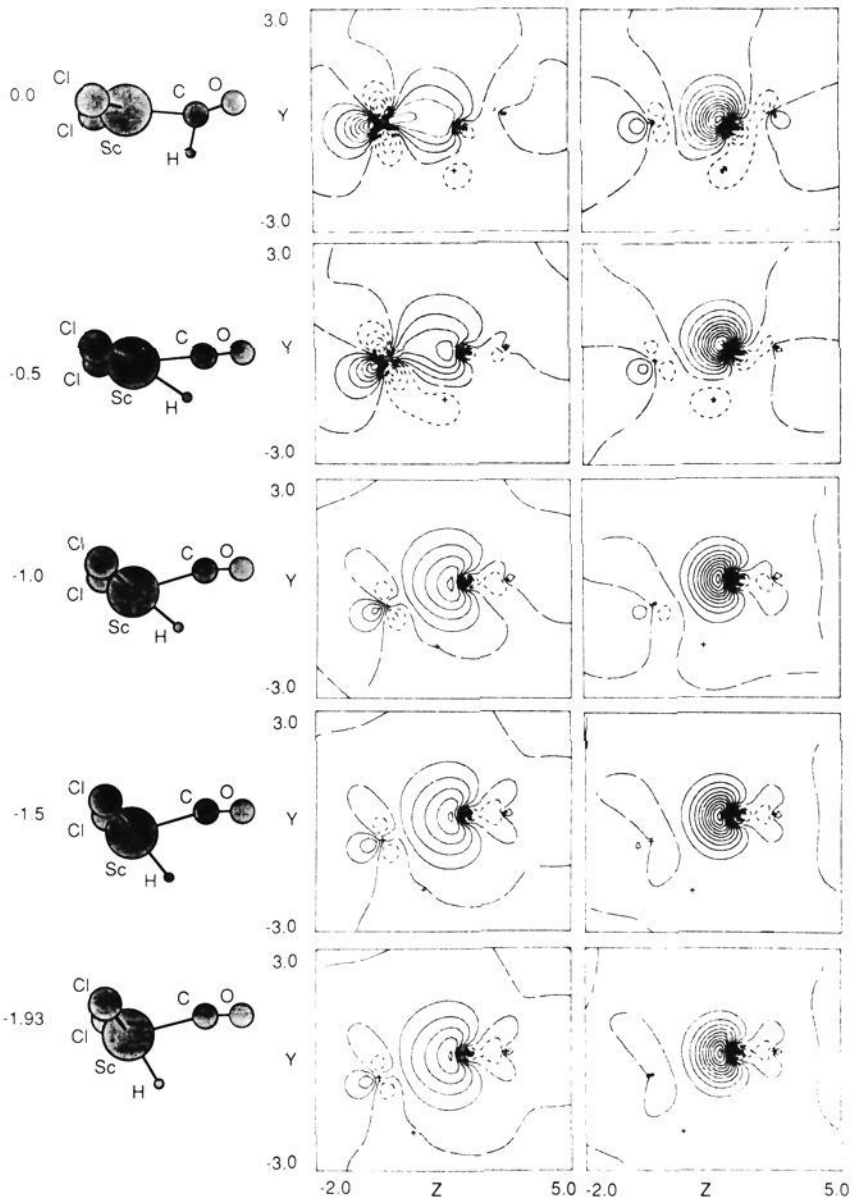

Figure 7. Contour plots of the GVB orbitals describing the formation of the C–H σ bond for the reaction coordinate connecting the reactant (plotted in Figure 2) and the transition state (plotted in Figure 4). The plotting plane and contours are as defined in Figure 2. The transition-state pair is plotted in the top row, the reactant pair is plotted in the last row, and points at 0.5-Å steps along the reaction coordinate are plotted in between.

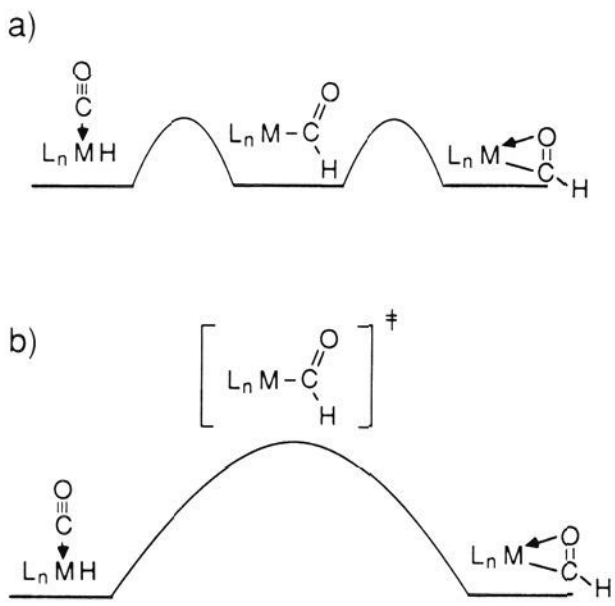

Figure 8. Schematic illustrations of the reaction coordinate connecting the reactant and the product η^2-formyl for (a) the normal case with an intermediate η^1-formyl and (b) the case were the intermediate η^1-formyl is a saddle point.

calization of the orbital in column 1 of Figure 14 onto the oxygen as the reaction proceeds. As discussed above in section II.B this increased delocalization provides a site for nucleophilic attack for the η^2-formyl product. The only changes in the remaining valence orbitals occur due the rotation of the formyl in going from η^1 to η^2.

III. Comparison with Other Work

The carbonyl insertion reaction is one of the most thoroughly studied organometallic reactions experimentally and theoretically.

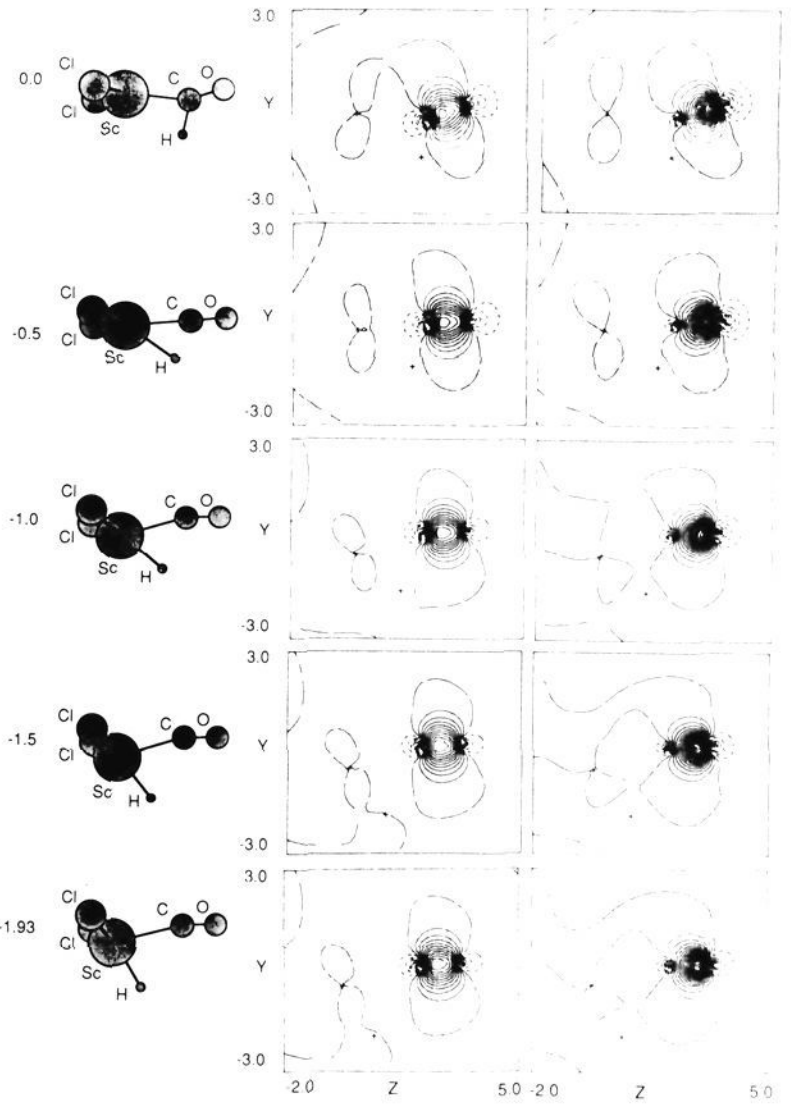

Figure 9. Contour plots of the GVB orbitals describing the changes in the C–O σ bond along the reaction coordinate connecting the reactant (plotted in Figure 2) and the transition state (plotted in Figure 4). The plotting plane and contours are as defined in Figure 2. The transition-state pair is plotted in the top row, the reactant pair is plotted in the last row, and points at 0.5-Å steps along the reaction coordinate are plotted in between.

The overall conclusions of the experimental efforts relevent to the present work were summarized in the introduction. Theoretically, the primary explanation for the low barrier of the reaction was first presented by Berke and Hoffmann[7] using extended Hückel theory. They attributed the low barrier ($\sim$20 kcal/mol for the alkyl insertion and $\sim$16 kcal/mol for the hydride insertion) to the stabilization of the $\sigma_{CO}-\sigma_{CH_3}$ acyl anion orbital by an unoccupied d orbital. For $Mn(CO)_4(CH_3CO)$ they found the η^2-acyl to lie energetically above the η^1-acyl form but there was no barrier along the reaction coordinate connecting the two acyl forms. The η^1-acyl was found to lie 18 kcal/mol above the methyl–carbonyl complex. Thus, the barrier for decomposition of the unsaturated η^1-acyl $Mn(CO)_4(CH_3CO)$ was calculated to be $\sim$2 kcal/mol. The observations by Berke and Hoffmann are in general agreement with experimental evidence on the $Mn(CO)_5CH_3$ system despite the reaction coordinate studied being an assumed one.

More recently there have been ab initio Hartree–Fock studies of the carbonyl insertion reaction for group 7 and 10 metal complexes.[11-13] The initial studies involved a partial geometry optimization along an assumed reaction coordinate.[11] Later Koga and Morokuma[12] studied the methyl insertion path using a palladium model complex $Pd(H)(PH_3)(CO)(CH_3)$ with a full geometry optimization of the transition-state structure. They found the transition state to be best described as resulting from a methyl migration rather than a carbonyl insertion. The transition state was found to lie 13.5 kcal/mol above the methyl carbonyl reactant and the acyl product to lie 8.8 kcal/mol above the methyl carbonyl reactant. Koga and Morokuma also investigated the effects of electron correlation on the energetics and found there to be a substantial lowering of the endothermocity and the barrier height using second-order Møller–Plesset perturbation theory (the energies quoted above are from the more accurate correlated calculations). Dedieu and Nakamura[13] have studied hydride insertion for $Mn(CO)_5H$ using a pointwise sequential optimization of the

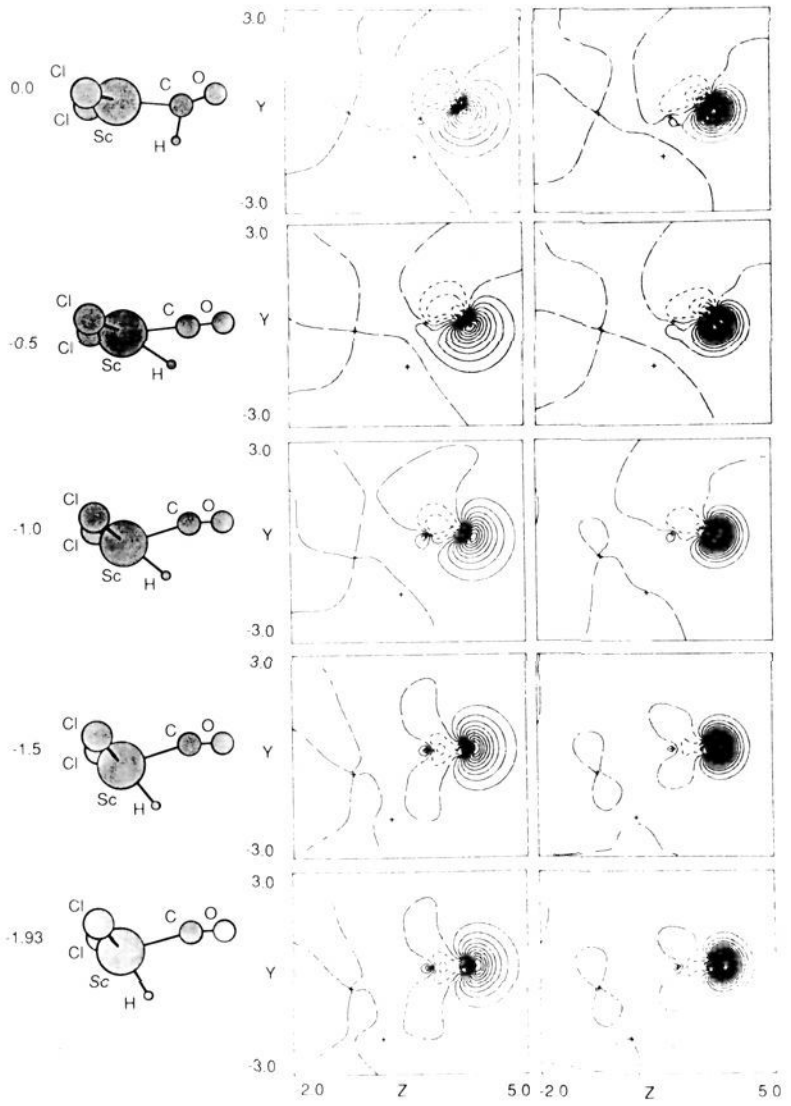

Figure 10. Contour plots of the GVB orbitals describing the conversion of the O s lone pair into an O sp lone pair along the reaction coordinate connecting the reactant (plotted in Figure 2) and the transition state (plotted in Figure 4). The plotting plane and contours are as defined in Figure 2. The transition-state pair is plotted in the top row, the reactant pair is plotted in the last row, and points at 0.5-Å steps along the reaction coordinate are plotted in between.

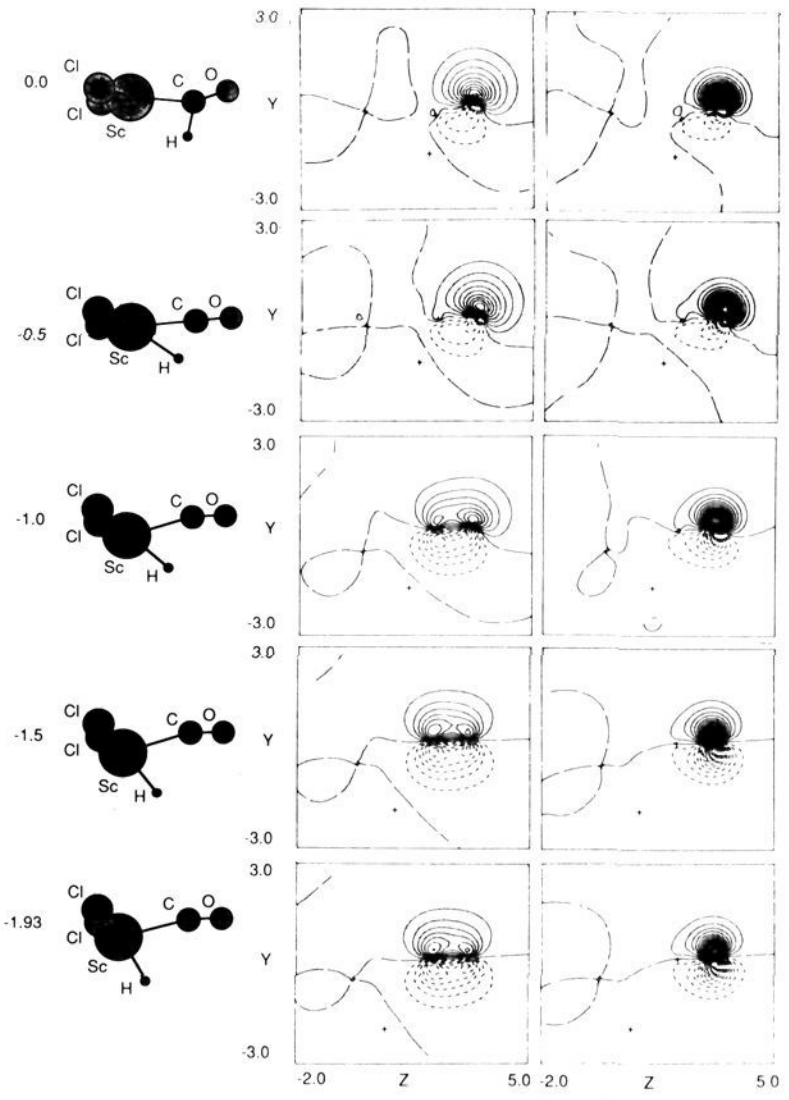

Figure 11. Contour plots of the GVB orbitals describing the conversion of the C–O π bond into an O sp lone pair along the reaction coordinate connecting the reactant (plotted in Figure 2) and the transition state (plotted in Figure 4). The plotting plane and contours are as defined in Figure 2. The transition-state pair is plotted in the top row, the reactant pair is plotted in the last row, and points at 0.5-Å steps along the reaction coordinate are plotted in between.

reaction coordinate. They found the transition state to be best described as resulting from a hydride migration rather than a carbonyl insertion. The transition state was found to lie 14.4 kcal/mol (HF) or 38.8 kcal/mol (CI) above the hydrido carbonyl reactant. The η^1-formyl product was calculated to be 10.4 kcal/mol (HF) or 38.4 kcal/mol (CI) above the hydrido carbonyl reactant.

Ziegler, Versluis, and Tschinke[9] have reexamined the carbonyl insertion path for $Mn(CO)_5R$ (R = H, CH_3) using the Hartree–Fock–Slater method. They found the η^1-formyl to lie 38 kcal/mol above the hydrido carbonyl and the η^1-acyl to lie 18 kcal/mol above the methyl carbonyl (in good agreement with the ab initio CI calculations of Nakamura and Dedieu[13]). They attributed the thermodynamic difference between the formyl and acyl to be due to a large difference between the Mn–H and Mn–CH_3 bond strengths. Using assumed reaction coordinates they found additional kinetic barriers of 1.4 and 2.6 kcal/mol for the hydride and methyl insertion reactions, respectively (again in good agreement with the ab initio CI calculations of Nakamura and Dedieu[13]). In contrast to the work of Berke and Hoffmann[7], Ziegler and co-workers[9] found the η^2 forms of the formyl and acyl complexes to be more stable than the η^1 forms by 16 and 19 kcal/mol, respectively.

Quite recently Axe and Marynick optimized the reaction coordinate for the $Mn(CO)_5CH_3$ system using PRDDO and then evaluated the energy along the reaction coordinate using ab initio Hartree–Fock. From the ab initio Hartree–Fock calculations they found the η^1-acyl to lie 10 kcal/mol above the methyl carbonyl (in disagreement with the ab initio CI calculations of Nakamura and Dedieu[13] and the HFS calculations of Ziegler and co-workers[9]). Using the PRDDO reaction coordinate they found an additional kinetic barrier of 7 kcal/mol for the methyl insertion reaction (in moderate agreement with the ab initio CI calculations of Nakamura and Dedieu[13] and the HFS calculations of Ziegler

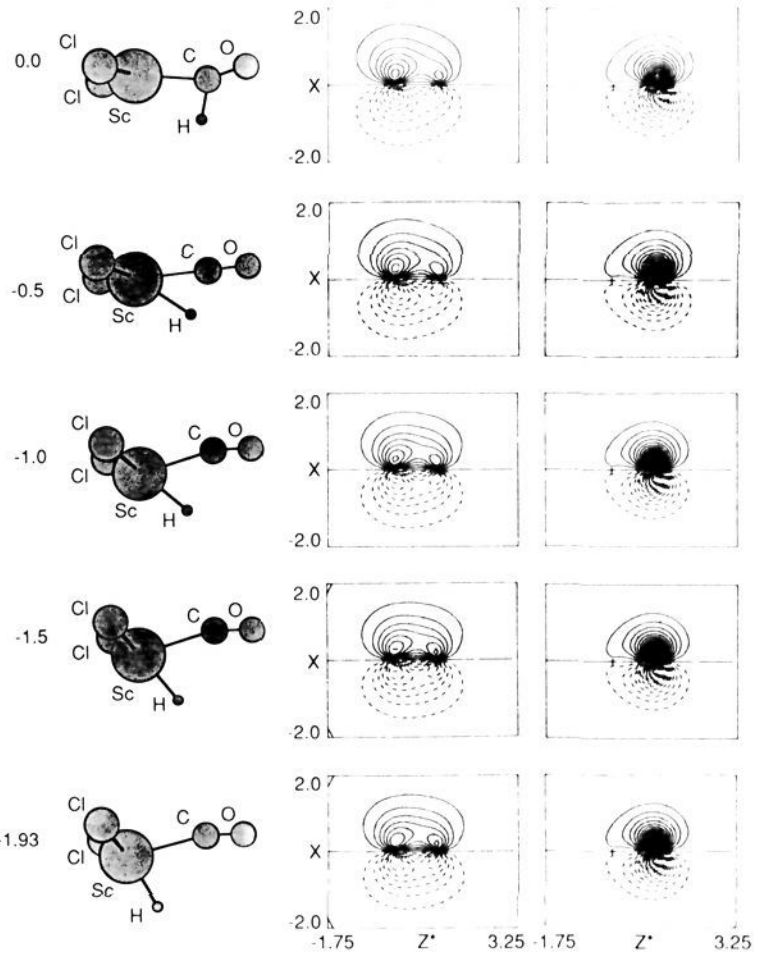

Figure 12. Contour plots of the GVB orbitals describing the changes in the perpendicular C–O π bond along the reaction coordinate connecting the reactant (plotted in Figure 2) and the transition state (plotted in Figure 4). The plotting plane and contours are as defined in Figure 2. The transition-state pair is plotted in the top row, the reactant pair is plotted in the last row, and points at 0.5-Å steps along the reaction coordinate are plotted in between.

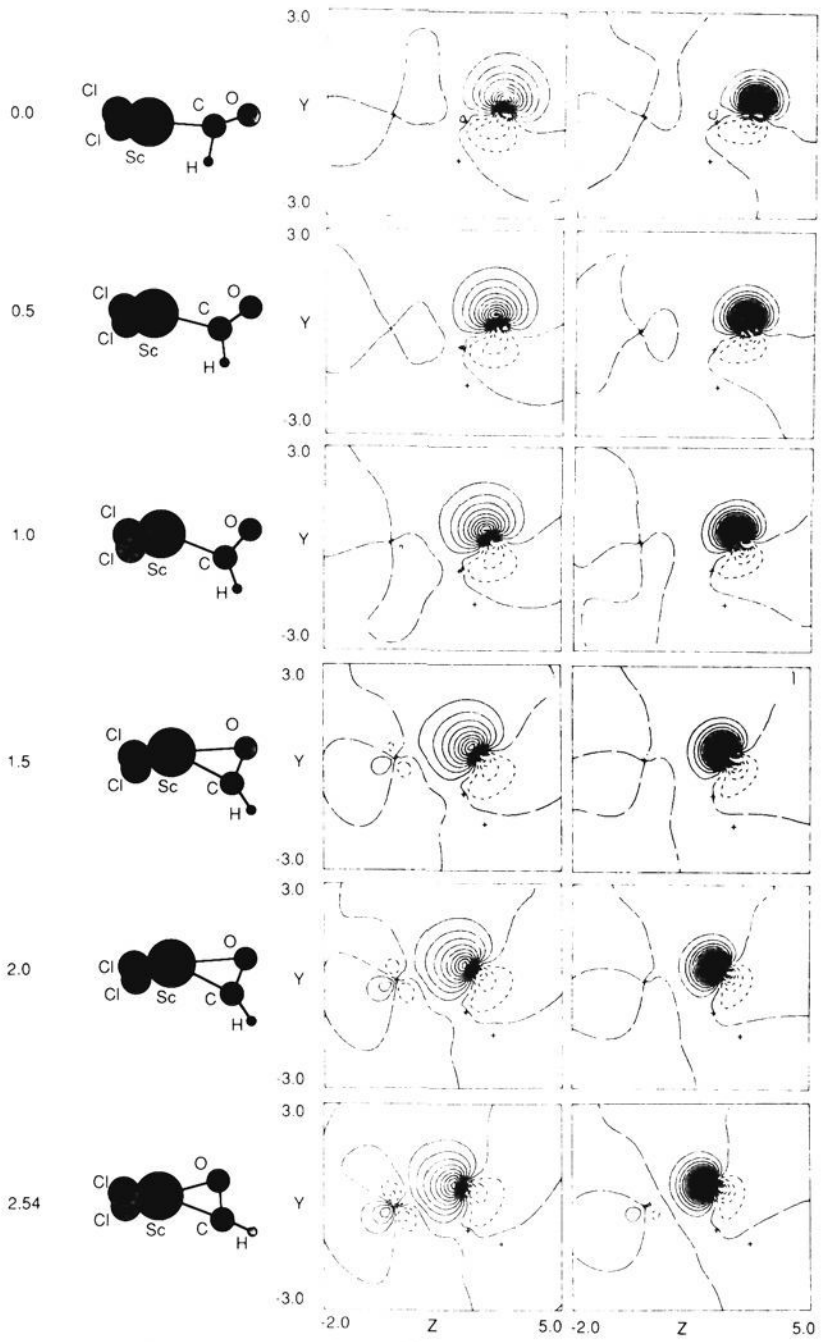

Figure 13. Contour plots of the GVB orbitals describing the gradual conversion of an O lone pair into a dative bond between O and Sc along the reaction coordinate connecting the transition state (plotted in Figure 4) and the η^2 product (plotted in Figure 3). The plotting plane and contours are as defined in Figure 2. The transition-state pair is plotted in the top row, the η^2 product pair is plotted in the last row, and points at 0.5-Å steps along the reaction coordinate are plotted in between.

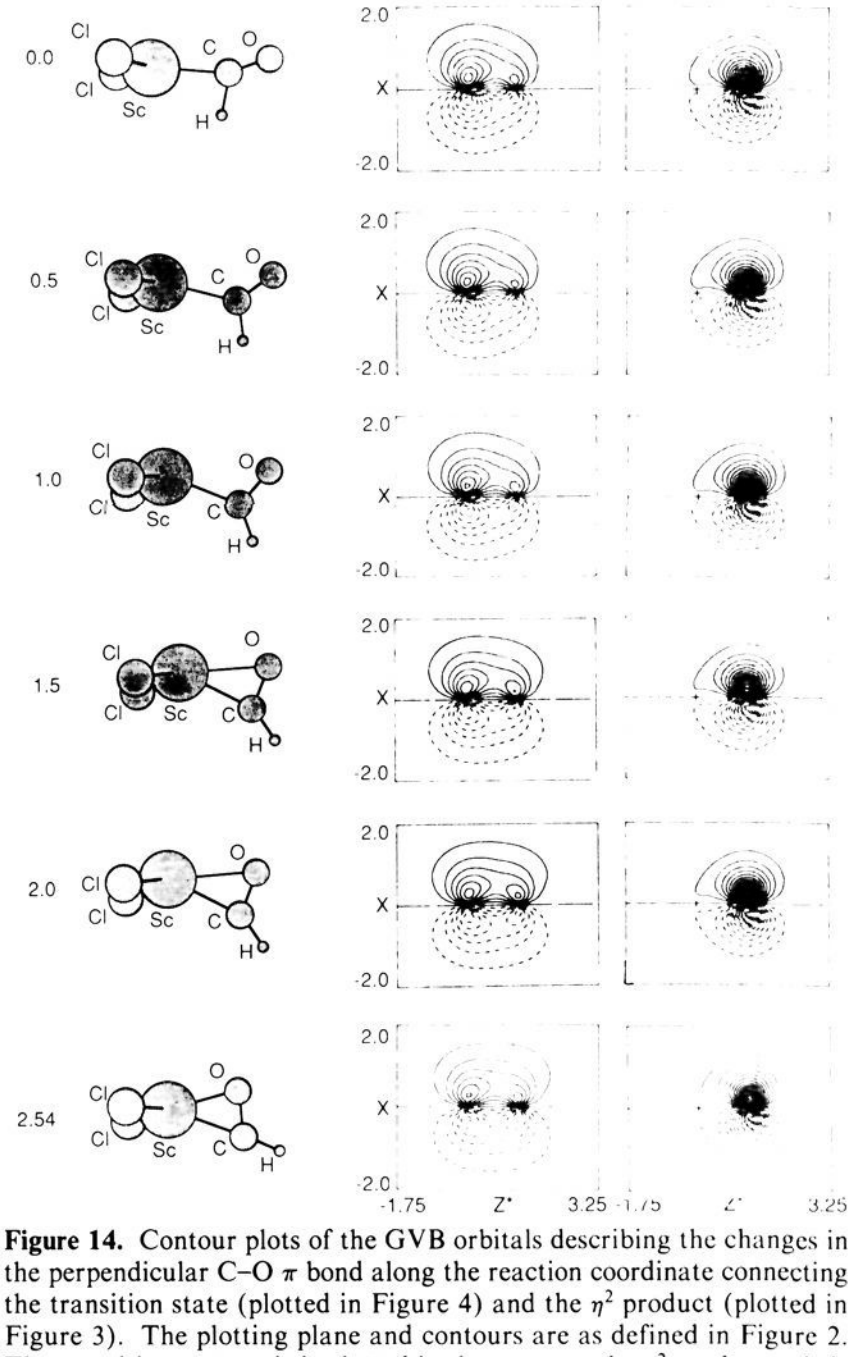

Figure 14. Contour plots of the GVB orbitals describing the changes in the perpendicular C–O π bond along the reaction coordinate connecting the transition state (plotted in Figure 4) and the η^2 product (plotted in Figure 3). The plotting plane and contours are as defined in Figure 2. The transition-state pair is plotted in the top row, the η^2 product pair is plotted in the last row, and points at 0.5-Å steps along the reaction coordinate are plotted in between.

and co-workers[9]). In contrast to the work of Berke and Hoffmann,[7] but in agreement with Ziegler and co-workers,[9] Axe and Marynick found the η^2 form of the acyl complex to be more stable than the η^1 form by 11 kcal/mol.

Experimental data on the $Mn(CO)_5CH_3$ system are not sufficient to differentiate between the theoretical results though matrix isolation studies tend to support the results of Hoffmann and Berke. That is, on photolysis of $Mn(CO)_5(CH_3CO)$ in a methane matrix the unsaturated species $Mn(CO)_4(CH_3CO)$ was formed.[18] The CO stretches for the acetyl group in the reactant and product were found to be most consistent with an η^1 formulation of the acetyl group. Decomposition of $Mn(CO)_4(CH_3CO)$ to $Mn(CO)_5CH_3$ was **not** observed. All of the theoretical reports to date are inconsistent with the observability of $Mn(CO)_4(CH_3CO)$. For each calculation the barrier to decarbonylation of $Mn(CO)_4(CH_3CO)$ was found to be quite small. This inconsistency can be rationalized by realizing that the matrix (CH_4) is likely to bind strongly enough to the site of unsaturation[19] to prevent conversion to either an η^2-acyl or to $Mn(CO)_5CH_3$. Thus, there is a need for more work on the $Mn(CO)_5CH_3$ system since in all of the theoretical studies either an assumed reaction coordinate or sequential pointwise optimization was used. Further, the explicit effect of the methane matrix needs to be studied theoretically.

Detailed theoretical studies on the electronic structure of η^2-formyl and -acyl complexes have appeared in the past year. Curtis, Shiu, and Butler[10] (using extended Hückel theory) find a delicate energetic balance between η^1 and η^2 complexes for Mo(II) complexes that is dependent on the shape of the ancilary ligands. Hoffmann and co-workers[8] also using extended Hückel theory reach the same conclusions for group 4 complexes. Our GVB description of the bonding of the scandium η^2-formyl is in agreement with the previous molecular orbital descriptions of the bonding of η^2-formyls and -acyls to transition metals.

The most significant difference between our work and the previous studies on the carbonyl insertion reaction is that we do not find the η^1-formyl to be a stationary state. The previous work focused on group 4 through group 10 complexes where additional ligand orbitals and/or d orbitals are likely to destabilize the η^2 form due to repulsive interactions between the O lone pair and the additional ligand orbitals and/or d orbitals, perhaps sufficiently to make the η^1 a stationary state. In addition, none of the previous studies on the group 4–6 species subjected the η^1-formyl or acyl species to either a gradient or force constant analysis. Thus, the structures found could well be unstable with respect to distortion of the coordinate defining the reaction coordinate connecting the η^1 species with the η^2 species, turning the η^1-formyl or -acyl into a point along the reaction coordinate rather than an equilibrium

(18) Hitam, R. B.; Narayanaswamy, R.; Rest, A. J. *J. Chem. Soc., Dalton Trans.* **1983**, 615–618.

(19) Perutz, R. N.; Turner, J. J. *J. Am. Chem. Soc.* **1985**, *97*, 4791. Demuynck, J.; Kochanski, E.; Veillard, A. *J. Am. Chem. Soc.* **1979**, *101*, 3467–3472. Welch, J. A.; Peters, K. S.; Vaida, V. *J. Phys. Chem.* **1982**, *86*, 1941–1947. Simpson, M. B.; Poliakoff, M.; Turner, J. J.; Maier, W. B.; McLaughlin, J. G. *J. Chem. Soc., Chem. Commun.* **1983**, 1355–1357. Rest, A. J.; Whitwell, I.; Graham, W. A. G.; Hoyano, J. K.; McMaster, A. D. *Ibid.* **1984**, 624–626.

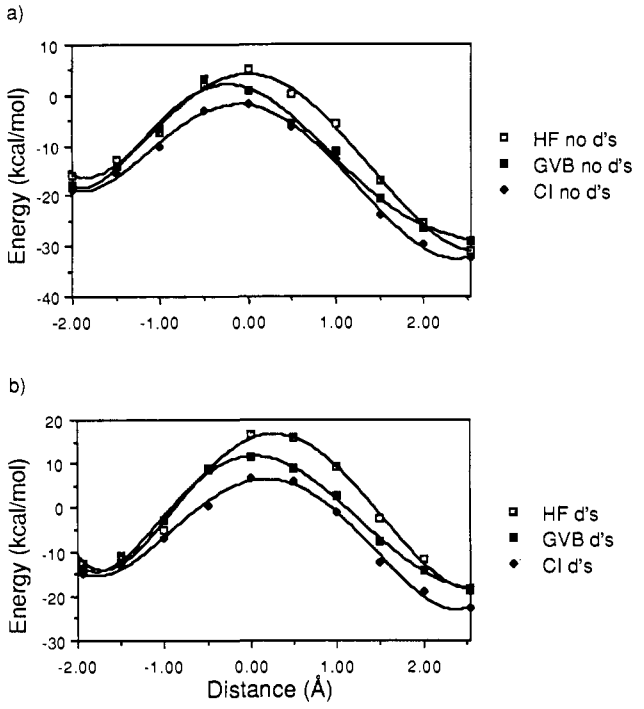

Figure 15. Calculated reaction profiles along the reaction coordinate. Hartree–Fock, generalized valence bond, and configuration interaction wave functions are plotted (a) without d polarization functions on carbon and oxygen and polarization functions on hydrogen and (b) with d polarization functions on carbon and oxygen and p polarization functions on hydrogen.

structure. Koga and Morokuma[12] did perform a full geometry optimization of the transition-state structure for the methyl insertion path for palladium. They found the transition state to be intermediate between the original methyl carbonyl and the η^1-acetyl product and the η^1-acetyl to be a stationary state.

IV. Summary

We find that carbonyl insertion into the Sc–H σ bond of Cl_2ScH occurs with a small activation energy ($\Delta E^{\ddagger}$ = 23.7 kcal/mol with respect to the Lewis acid–base adduct) forming an η^2-formyl complex without the intermediacy of an η^1-formyl complex. The overall reaction is found to be moderately exothermic (ΔE = −6.1 kcal/mol with respect to the Lewis acid–base adduct). The explanation for the small barrier is the same as for previously studied metallo 4-center 2 + 2 reactions. There are differences due to the instability of the η^1-formyl and the localization of one of the pairs of electrons in the reactant on a single center. Overall agreement with previous theoretical work is found and electron correlation and polarization functions in the basis are found to affect the energetics of the reaction but not substantially alter the geometric position of the saddle point.

V. Calculational Details

A. Basis Sets and Effective Potentials. All of the calculations reported here were carried out with use of Cartesian Gaussian basis sets. For Cl[20] an effective potential was used to replace the core electrons allowing self-consistent orbital optimization to be carried out only for the valence electrons. For Sc[21] an effective potential was used to replace the 1s, 2s, and 2p orbitals, again reducing the number of functions for the self-consistent orbital optimization. For geometry optimizations (7s,4p/3s,3p) basis sets were used for carbon and oxygen.[22] A (6s/3s) basis, unscaled, was used for hydrogen.[23] For the final series of calculations along the reaction coordinate the Dunning–Huzinaga[24] valence double-ζ carbon and oxygen basis sets were used, augmented with sets of d Gaussians (ζ = 0.75 and 0.87 for carbon and oxygen, respectively).[24] The hydrogen basis was augmented with a single set of p Gaussians (ζ = 0.6) for the final series of calculations along the reaction coordinate. For chlorine, a valence minimum basis (3s,3p/1s,1p)[20] was used for all calculations. For Sc, a valence double ζ (6s,5p,5d/3s,3p,2d) basis[21,25] was used for all calculations.

B. Wave Functions. The geometries of the stationary points as well as the mass-weighted Cartesian coordinate steepest descent paths from the transition state to the reactant and to the product were generated with analytic gradient techniques with use of Hartree–Fock wave functions. For the final optimized geometries, GVB(6/12) wave functions[26] were obtained and CI calculations[27] were performed consisting of RCI quadruples plus a Pol(2/1)-CI[28] including the GVB orbitals and the entire virtual space. For each structure all of the valence electrons associated with Sc, H, C, and O were explicitly correlated.

C. Geometries. In order to minimally bias the geometric results, geometry optimizations were started from reasonable guesses for complexed carbon monoxide, the transition state leading to formation of an η^1-formyl, the η^1-formyl itself, and an η^2-formyl. The lack of a stationary state associated with an η^1-formyl was confirmed with a determination of the reaction coordinate with use of a steepest descent path in mass-weighted Cartesian coordinates. When a hand optimization of the geometry was used, the η^1-formyl was found to lie approximately 0.8 Å along the reaction coordinate connecting the saddle point and the η^2-product.

D. Reaction Coordinate. In order to assess the effects of electron correlation and polarization functions on the reaction profile Hartree–Fock, generalized valence bond, and configuration interaction calculations were performed with and without polarization functions on C, O, and H for ten points along the reaction coordinate. As would be expected inclusion of electron correlation decreases the barrier height (see Figure 15). Addition of polarization functions increases the barrier height (compare Figure 15a with Figure 15b). There are also basis set effects on the overall exothermicity of the reaction. For each wave function polarization functions are more important for the reactants; the exothermicity is decreased between 7 and 11 kcal/mol. With polarization functions included electron correlation only has a 2-kcal/mol effect on the exothermicity. As mentioned above, Koga and Morokuma[12] also investigated the effects of electron correlation on the energetics of the carbonyl insertion reaction and found there to be a substantial lowering of the endothermocity and the barrier height using second-order Møller–Plesset perturbation theory.

Acknowledgment. This work is supported by NSF Grant CHE-8405399. Acknowledgment is made to the CSU Supercomputing Project for partial support of this research.

(20) Rappé, A. K.; Smedley, T. A.; Goddard, W. A. *J. Phys. Chem.* **1981**, *85*, 1662–1666.
(21) Hay, P. J.; Wadt, W. r. *J. Chem. Phys.* **1985**, *82*, 270–283.
(22) Rappé, A. K.; Goddard, W. A., manuscript in preparation.
(23) Huzinaga, S. *J. Chem. Phys.* **1965**, *42*, 1293.
(24) Dunning, T. H.; Hay, P. J. In *Modern Theoretical Chemistry: Methods of Electronic Structure Theory*; Schaefer, H. F., III, Ed.; Plenum: New York, 1977; Vol. 3, Chapter 1, pp 1–27.
(25) Rappé, A. K.; Smedley, T. A.; Goddard, W. A. *J. Phys. Chem.* **1981**, *85*, 2607–2611.
(26) Bobrowicz, F. W.; Goddard, W. A. In *Modern Theoretical Chemistry: Methods of Electronic Structure Theory*; Schaefer, H. F., III, Ed.; Plenum: New York, 1977; Vol. 3, Chapter 4, pp 79–127.
(27) Shavitt, I. In *Modern Theoretical Chemistry: Methods of Electronic Structure Theory*; Schaefer, H. F., III, Ed.; Plenum: New York, 1977; Vol. 3, Chapter 6, pp 189–275.
(28) Hay, P. J.; Dunning, T. H. *J. Chem. Phys.* **1976**, *64*, 5077.